AUT Journal of Electrical Engineering
10.22060/EEJ.2026.24491.5713

Optimized Battery Charging System for Electric Vehicle with Proportional Integral Controlled High Frequency Resonant Bridgeless Power Factor Correction Converter

Challa Leela Kumari[1*], Dondapati Ravi Kishore[2], Kailash Kumar[3], Nikhil Kumar[4], Md Shahil[5]

[1]Assistant Professor, Department of Electrical and Electronics Engineering, Godavari Institute of Engineering and Technology (A), Rajahmundry, India.

[2]Professor, Department of Electrical and Electronics Engineering, Godavari Global University, Rajahmundry, India.

[3,4,5] UG Scholar, Department of Electrical and Electronics Engineering Godavari Institute of Engineering and Technology (A), Rajahmundry, India.

*Corresponding author Email: leesmileschalla2021@gmail.com

Abstract:

The goal of research is to develop an optimized Electric Vehicle (EV) charging system with enhanced efficiency and cost-effectiveness by integrating a High Frequency Resonant Bridgeless (HFRB) Power Factor Correction (PFC) converter and a Proportional Integral (PI) controller. To attain the goals, the subsequent tasks are proficient: a novel Bridgeless PFC converter is developed to improve power factor correction and power quality; a PI controller is exploited to control output voltage with reduced implementation and maintenance costs and a Pulse Width Modulation (PWM) generator within a Hysteresis Current Controller (HCC) is deployed to enhance current protection, system stability, and fault tolerance. The system is validated using MATLAB/Simulink-based simulations. The significant outcomes are the accomplishment of a high charging efficiency of 97%, improved power quality, reduced heat generation, and enhanced system control operations. The significance of obtained results is that the proposed system ensures optimized EV battery charging with increased reliability, reduced implementation costs, and robust fault tolerance, contributing to the development of effective EV charging infrastructure.

Keywords:

EV, HFRB-PFC converter, PI, PWM and Hysteresis Current Controller (HCC)

Notation List

V_S	Input voltage
f_L	AC line frequency
V_O	Output voltage
V_{o1} and V_{o2}	Voltage across V_{C1} and V_{C2}
k	Resonant inductors ratio
G	Voltage gain
f_S	Switching frequency
$\widehat{V_S}$	Highest value of sinusoidal input voltage
i_{error}	Current error
i_{Aref}	Reference current
i_A	Measured current

1. Introduction

In recent days, large number of EV's are undergoing various developments in order to attain enhanced EV charging performance [1-2]. However, attaining better EV charging still faces certain difficulties associated with the higher requirements of power quality for EV charging [3-4]. Several measures utilized, obtained AC power form the source, rectified using uncontrolled rectifier bridge and fed directly to the EV charging load, thereby leading to reduced power factor within the charging system [5-6]. Thus, reduced power factor leads to increased harmonic distortion in current [7-8]. In spite of this, to address this issue and to obtain improved, convenient and timely charging of EV battery, PFC plays as essential role [9-10].

In conventional PFC converter, semiconductor device causes certain conduction losses, thus to reduce these conduction losses, bridge rectifier plays a crucial part at the input phase, thus increasing the system efficiency [11-12]. The integration PFC enables to acquire filtering and rectification of the obtained AC power by providing power factor correction [13].

However, due to larger power requirements of the EV battery, during insufficient voltage and high current supply, Rectifier Bridge undergoes higher loss which cannot be easily ignored [14-15-16]. Henceforth, various PFC approaches are considered to attain improved EV battery charging. Initially, Bridgeless – Boost converters are considered due to it simple and easy integration. However, these converters struggled with reduced voltage output. In [17] the authors innovated PFC converter and it attains reduced switching losses with upgraded power quality, thus improving the overall efficacy of the PFC but struggled with reduced efficiency during low power circumstances.

Significantly, authors in [18] introduced Buck-Boost PFC AC-DC converter for attaining control of battery charger for low voltage EV. Nevertheless, it increases the system complexity. In addition to this, [19] utilizes a discontinuous Current Conduction Mode (DCM) BL PFC converter for attaining natural PFC for AC input. The implementation of DCM with PFC protects the input voltage and current, providing reliable and robust converter performance. Nonetheless, this technique is not suitable for larger EV applications as it provides reduced efficiency during high power situations.

Henceforth, this paper suggests a High Frequency Resonant Bridgeless PFC converter for overcoming above mentioned shortcomings and to attain effective charging of EV. The foremost framework and objectives are,

- To attain enhanced power factor correction and power quality output for effective EV charging, High Frequency Resonant Bridgeless PFC converter is deployed.
- To ensure improved current security with enhanced fault tolerance, PWM generator with HCC is utilized, which increases the system reliability.

- To regulate the output voltage, PI controller is implemented which attains easy and simple integration with reduced expenses providing efficient and reliable control approach.

2. Proposed Modelling

Fig. 1 illustrates block diagram of optimized Battery Charging System for EVs. The major objective of this system is to attain high-frequency power conversion for improved charging of EV.

Initially, input AC supply is fed to high frequency resonant bridgeless PFC converter which enables power factor correction. Power factor correction is achieved by affiliating input current with input voltage, minimising power losses attaining seamless conversion of AC to DC making it suitable for EV charging.

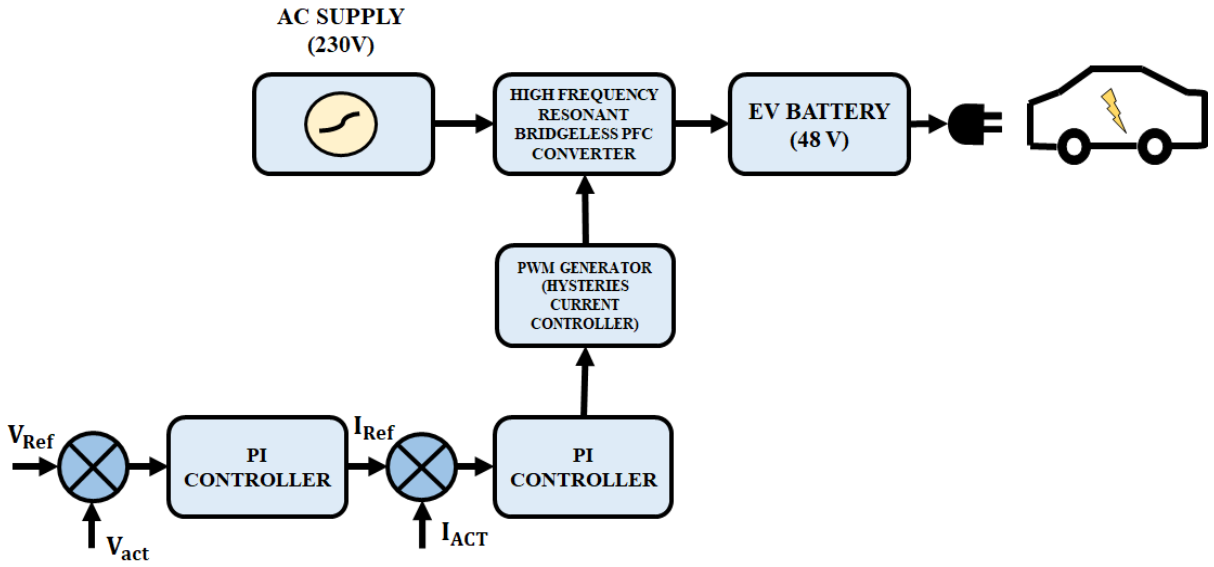

Fig. 1. Block Diagram of Optimized Battery Charging System for EVs

In addition to this, for enhanced PFC converter performance, PWM generator with hysteresis controller and PI controller is utilized. Secondly, PWM generator produces switching pulses for controlling PFC converter, attaining effective and regulated output voltage and current. Furthermore, PI controller, compares the reference voltage with actual voltage and adjust PWM generator consequently. Finally, the output from PFC converter is directly fed to EV for charging. Therefore, the proposed system as a whole ensures to attain optimized EV charging with increased reliability and stability.

10.22060/EEJ.2026.24491.5713

2-1- Modelling of high frequency resonant bridgeless PFC converter

Circuit of resonant PFC converter is depicted in Fig. 2, input voltage together with LC filter is termed as V_s. In this approach, switch S_1 with diode D_1 and D_{o1} is kept ON in the positive half cycle. Similarly, in negative half cycle, D_2 and D_{o2} is activated. In order to prevent, system short circuit due to input voltage source, external series of diode is considered essential for switch S_1 and S_2. Henceforth, the gating signals for both switches are applied concurrently without utilizing any sensors for sensing positive and negative half cycles.

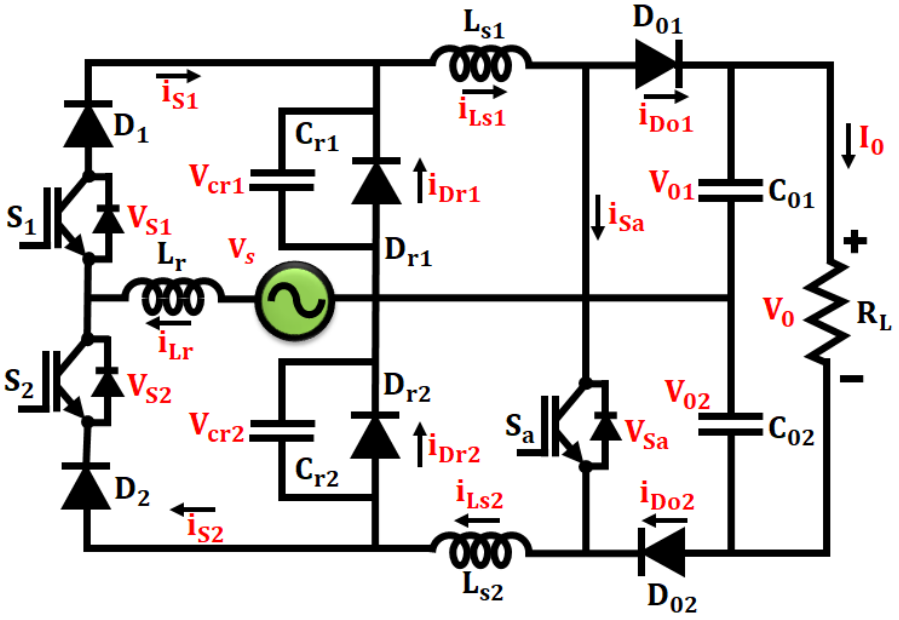

Fig. 2. Circuit Diagram of high frequency BL-PFC converter

In the positive half cycle, converter acts in 2 different modes, mode A, where the input voltage V_s is higher than that of $V_o/2$. Significantly, during mode B, V_s is lightly lesser than $V_o/2$, thus, energy transmission is blocked and null crossing distortion is attained at the input current because of gathered energy on C_1. Due to this reason, S_a is kept in ON state, hence, the collected energy is transferred to output resonant inductors L_1 and L_2. Afterwards, this energy is discharged by turning OFF S_a and Fig. 3 showcases the switching waveform of both stgaes.

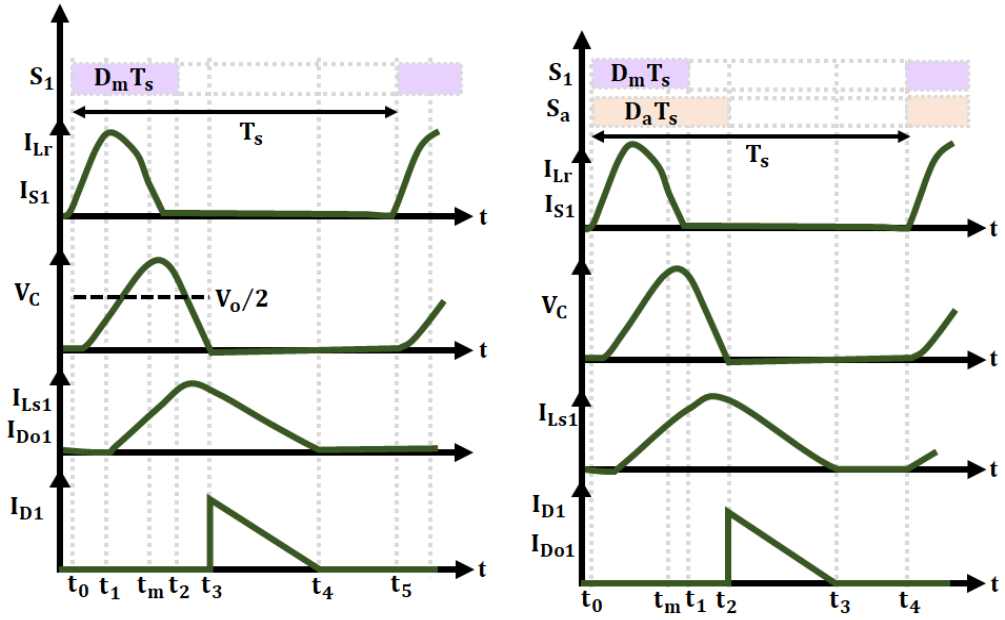

Fig. 3. Switching Waveforms (a) Mode A (b) Mode B

Operating Modes:

For positive half cycle, f_s is higher than f_L. Henceforth, V_s attains consistent switching cycle. Similarly, the voltage on output side is also regarded as stable as C_{o1} and C_{o2} are significantly larger. Due to the symmetrical structure, $V_{o1} = V_{o2} = V_o / 2$, $C_1 = C_2$ and $L_1 = L_2 = L_s$. Where, the voltage across V_{C1} and V_{C2} are V_{o1} and V_{o2}.

To further, simplify working modes equations, k and G is expressed as,

$$k = \frac{L_s}{L_r} \tag{1}$$

$$G = \frac{V_o}{2\hat{V}_s} \tag{2}$$

Where, $\hat{V}_s$ represents the sinusoidal input voltage's highest value.

10.22060/EEJ.2026.24491.5713

$$V_s = \hat{V}_s \sin\left[\omega_g t\right] \tag{3}$$

Operating mode A: During this mode, switch S_a is turned OFF, and mode A is further divided into five different time intervals.

Interval 1: At t_0, S_1 is kept in ON condition, thus C_1 gets charged via V_s. Whereas, C_{o1} and C_{o2} provides energy to R_L.

$$V_{Cr1}(t) = V_C(t) = \hat{V}_s\left(1 - \cos\left[\omega_{r1}\left(t - t_0\right)\right]\right) \tag{4}$$

$$I_{Lr}(t) = \frac{\hat{V}_s}{Z_{r1}} \sin[\omega_{r1}(t - t_0)] \tag{5}$$

Here, $\omega_{r1} = 2\pi / T_{r1} = 1/\sqrt{L_r . C}$ and $Z_{r1} = \sqrt{L_r . C}$. At t_1, V_{C1} reaches $V_o / 2$, hence, I_{Lr} during t_1 is,

$$I_{Lr}(t) = I_1 = \frac{\hat{V}_s}{Z_{r1}} \sqrt{G(2 - G)} \tag{6}$$

Where,

$$t_1 = t_0 + \frac{1}{\omega_{r1}}\left(\pi - cos^{-1}\left[G - 1\right]\right) \tag{7}$$

Where, the voltage and current across C_{r1} *and* C_r are V_{Cr} and I_{Cr}. By solving the capacitor voltage charging expression for t_1 at V_{C1} is similar to half of V_O, the equation(7) is obtained.

Interval 2: During this interval, D_{o1} is turned ON which in turn produces a resonant loop consisting L_1 and C_1. Here, C_1 gets charged using t_1 to t_m. Later, C_1 energy is transferred to R_L during t_m to t_2 through L_{s1}.

Interval 3: S_1 is kept OFF, while C_1 releases into load in resonant manner, which continues until V_{C_1} becomes zero and D_1 gets turned ON.

Interval 4: At t_3, D_1 is kept in ON state and $V_o/2$ positioned across L_1, hence, current is minimized linearly.

Interval 5: At t_4, all the semiconductors are turned OFF, thus, C_{o1} and C_{o2} provide the load and, the positive cycle ends and the negative cycle begins. Fig. 4 depicts the various working modes of proposed converter.

Operating mode B: To balance input current's zero distortion, gating signal S_a is applied. Furthermore, functioning mode B is again divided into four different intervals and are operate in similar manner of operating mode A. To further attain improved current control with rapid response rate, PWM generator in HCC is utilized. The integration of PWM in HCC achieves enhanced efficiency and reliability with rapid dynamic response rate.

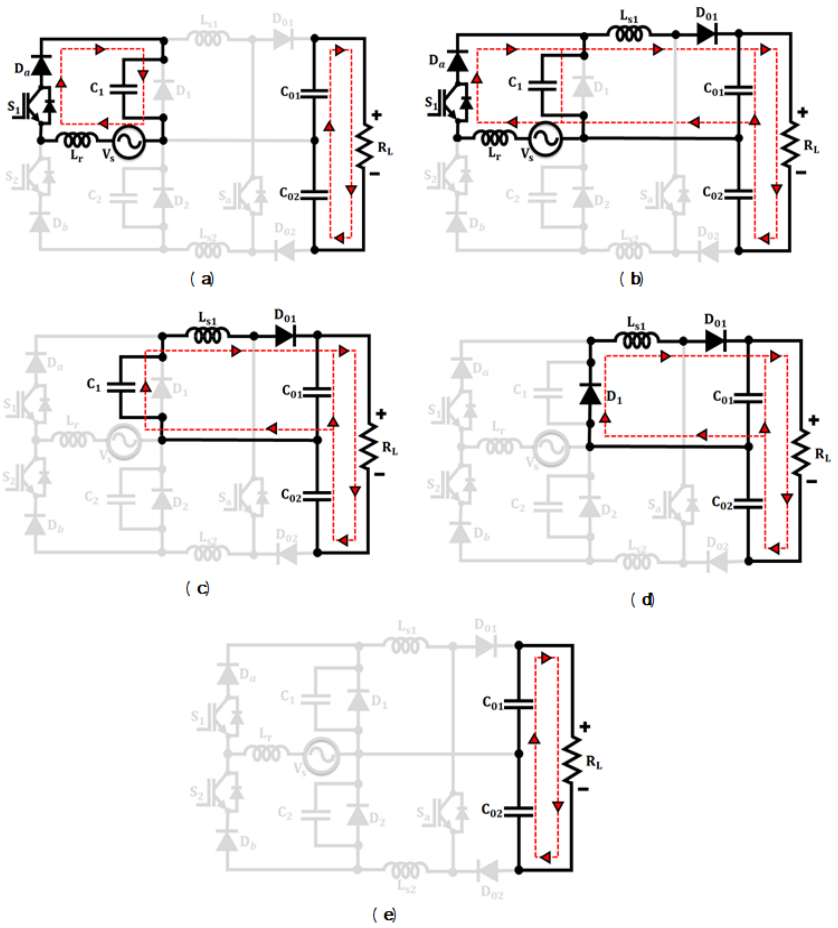

Fig. 4. Circuit Diagram of five intervals in operating mode A with S is inactive

10.22060/EEJ.2026.24491.5713

2-2- Modelling of PWM generator in HCC

The HCC approach is vitally utilized due to its simplicity, enhanced current defence, quick dynamic response and increased tolerance towards parameter variations. The block of hysteresis current control in illustrated in Fig. 5.

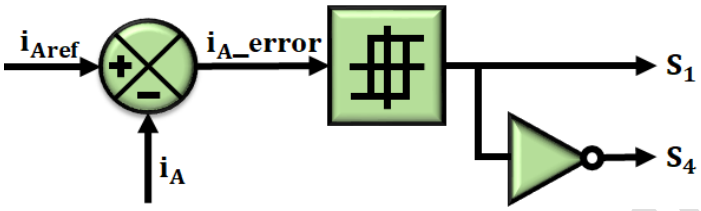

Fig. 5. Block diagram of HCC [20]

The current error (i_{error}) is designed by deducting (i_{Aref}) and (i_A). The obtained error is further compared to the hysteresis band to produce the switching pulses. The hysteresis control constrains current in band and bandwidth value (h) is kept stable. The current error is determined using,

$$i_{A\_error} = i_{Aref} - i_A \tag{8}$$

The lower and upper hysteresis band is compared using the hysteresis current controller,

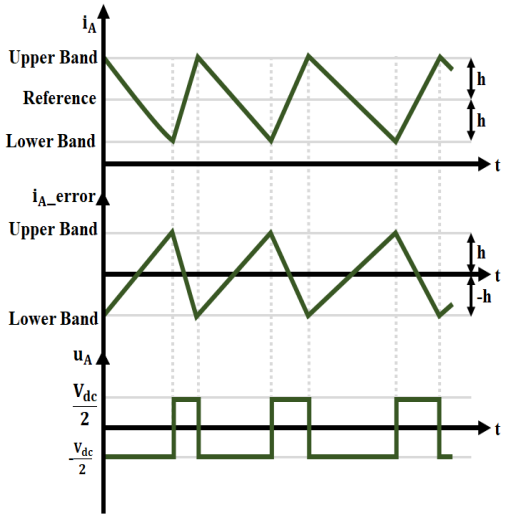

Fig. 6. PWM generation in HCC [20]

If $i_{A\_error} > +h$ then, i_A increases and if $i_{A\_error} < -h$ then, i_A decreases, the hysteresis current control along with the PWM generation is shown in Fig. 6. Moreover, PI controller is deployed to improve the control performance by removing steady state errors, thus increasing the system stability.

2-3- Modelling of PI controller

PI controller is often utilized for rectifying the errors acquired between actual and desired value of developed system. PI controller is the combination of proportional and integral controller which is utilized generally in control system for consistently altering the output based on error signal. Transfer Function of PI controller is evaluated using,

$$G_{PI}(s) = K_p + \frac{K_i}{s} \tag{9}$$

Where, K_p represents the proportional constant and K_i denotes integral constant. Fig. 7 represents PI controller's equivalent circuit.

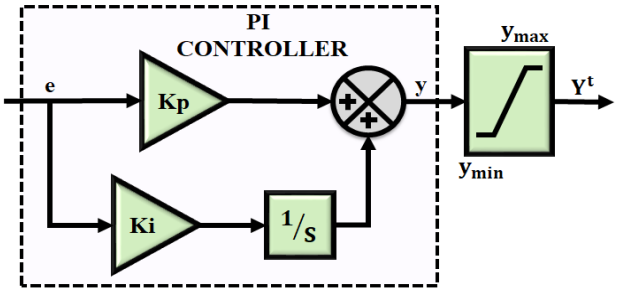

Fig. 7. Equivalent circuit diagram of PI controller [21]

The output generated by the PI controller is expressed as,

$$u(t) = K_p\, e(t) + K_I \int e(t)\, dt \tag{10}$$

Where, $e(t)$ denotes the error signal. Overall, the developed system ensures to attain improved battery charging with optimum control.

10.22060/EEJ.2026.24491.5713

3. Results and Discussion

This part deals with evaluation and analysis of PI controlled high frequency resonant BL PFC converter using MATLAB/Simulink along with their comparative analysis discussed in terms of their power factor and efficiency. The specification of parameters are added in Table 1.

Table 1. Specification of parameters

Parameter	Specification
AC Source	
Source current	20 A
Source voltage	220 V
high frequency BL-PFC converter	
L_{s1}, L_{s2}	4.7 mH
C_1, C_2	22 μF
C_{01}, C_{02}	2200μF
Switching Frequency	10 kHz

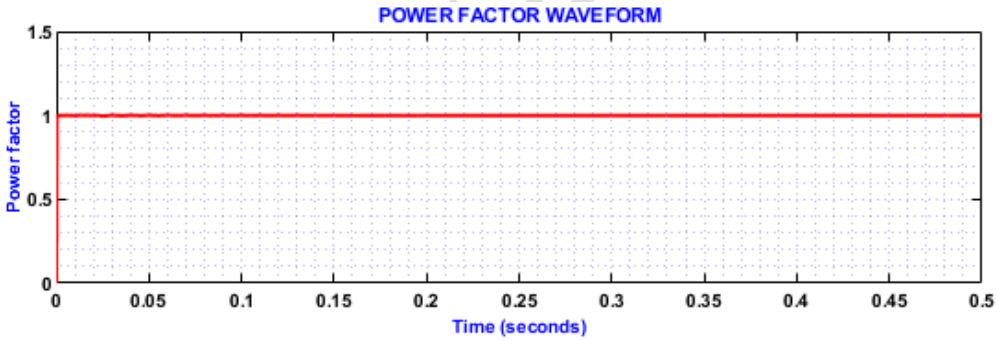

Fig. 8. Waveform of Power Factor

Fig. 8 represents the power factor waveform, in which power factor remains stable at 1 (unity) throughout the entire time period. Indicating, efficient functioning of developed system with reduced power losses and minimized overheating issues.

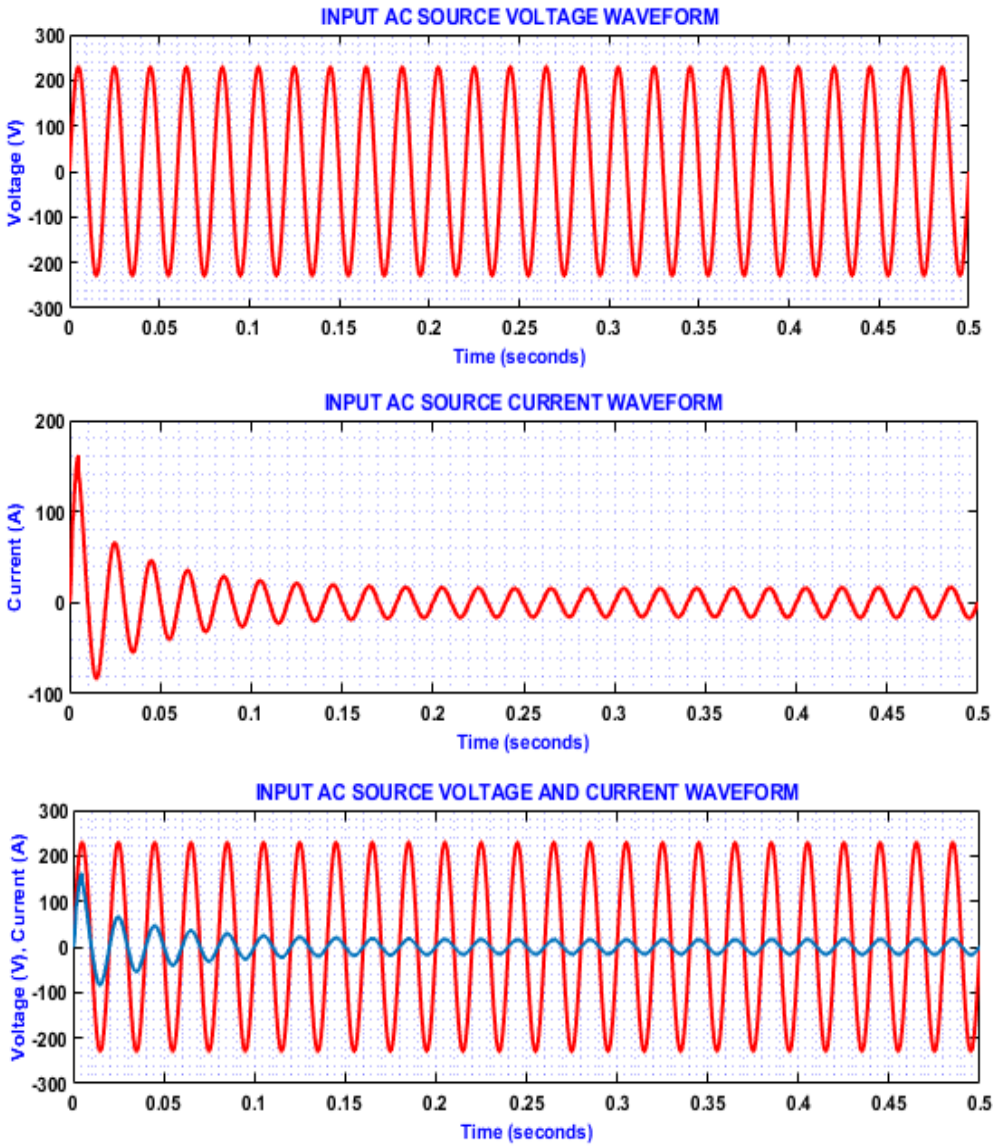

Fig. 9. Waveform of Input AC source Current and Voltage

Fig. 9, the first graph implies the input AC source voltage waveform, where the input voltage remains stable between ±220 V, thus ensuring reliable and consistent power supply. Similarly, second graph indicates the input AC source current waveform, in which current initially fluctuates and then stays stable, thereby, enhancing system efficiency. The third graph refers to both voltage and current waveform, where both the current and voltage exhibit perfect synchronization, hence providing effective utilization of real power with reduced reactive power.

10.22060/EEJ.2026.24491.5713

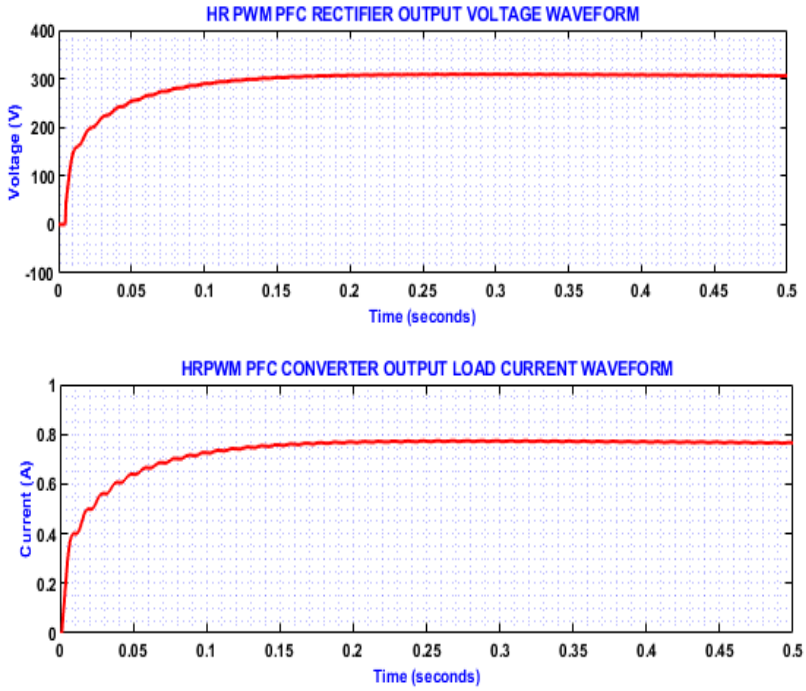

Fig. 10. Rectifier output voltage and converter current Waveform

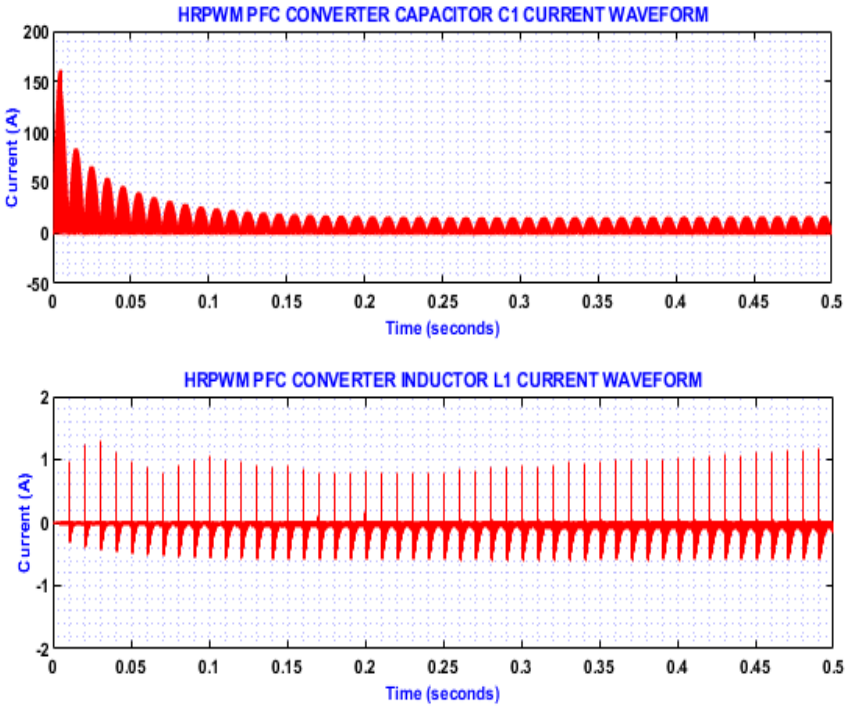

Fig. 11. Converter capacitor current and converter inductor current waveform

Fig. 10 represents the HR PWM PFC rectifier output voltage waveform and HR PWM PFC converter output load current waveform, where both the output voltage and current gradually increases and further stays stable at 300V and 0.7 A respectively. Fig. 11 implies the current waveform for HR PWM PFC converter through capacitor C_1 and inductor L_1, the first graph represents that, rapid increase in current which further stabilizes through the given time duration. Similarly, the second graph indicates that, the current through inductor initially fluctuates and later stays consistent indicating effective system functioning. The output power of 150 W is attained by this converter.

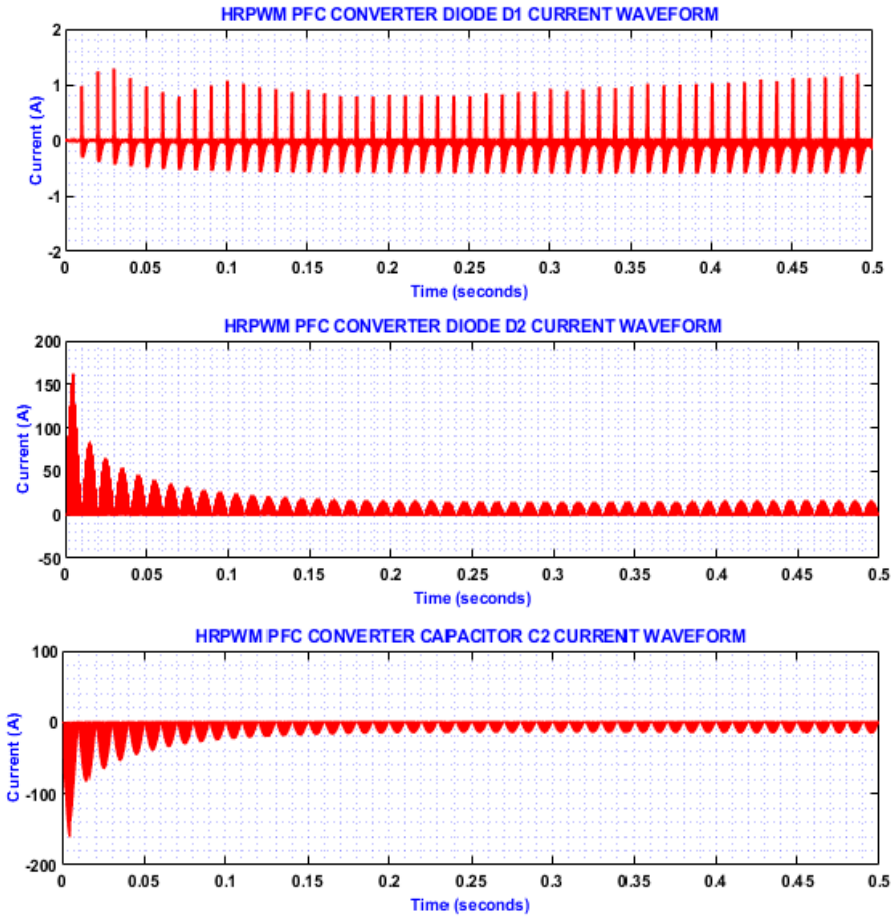

Fig. 12. Converter diode current and capacitor current waveform

Fig. 12 represents three graph comprising HR PWM PFC converter diode D_1, D_2 and capacitor C_2 current waveform. The current through diode D_1 keeps deviating while, the current through diode D_2 initially

10.22060/EEJ.2026.24491.5713

rapidly increase and further stabilizes. Moreover, current through capacitor C_2 implies that, stable current thus, indicating enhanced system reliability.

Case 1 → Input Voltage – 220 V

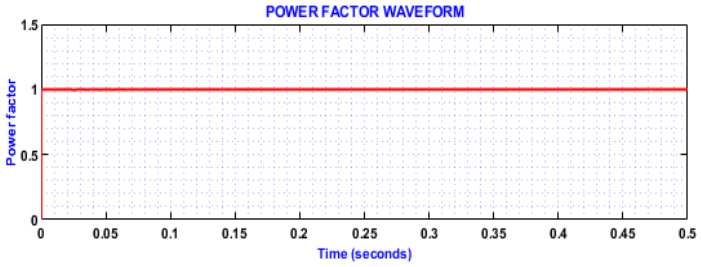

Fig. 13. Waveform for Power Factor

Fig. 13 indicates the waveform of power factor in which the power factor remains at 1 unity throughout the given time duration even with input power 220V, indicating effective system performance with varying input voltage.

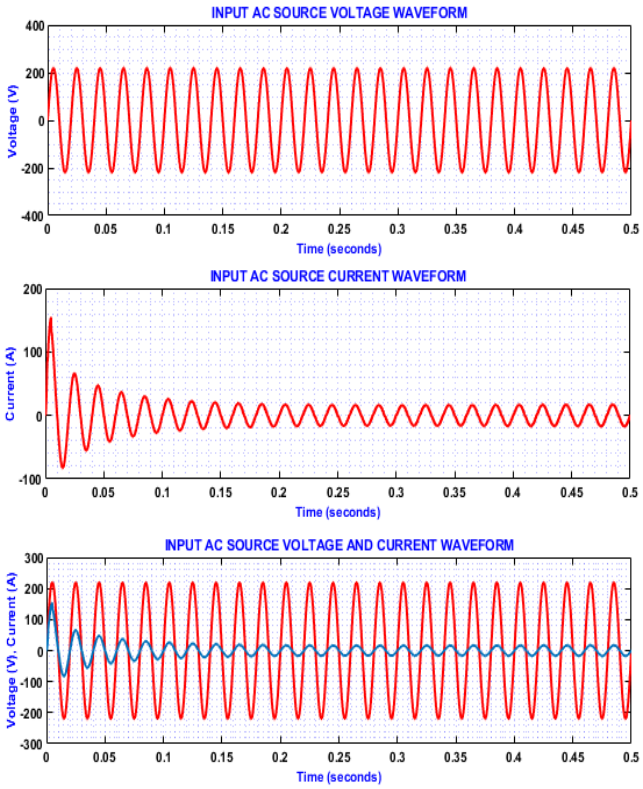

Fig. 14. Waveform of AC source current and voltage

Fig. 14 implies the AC source current and voltage waveform, where voltage remains consistent between ±200V and current waveform showcases that, current initially fluctuates and steadied. Significantly, third graph depicts that, faultless synchronization of voltage and current.

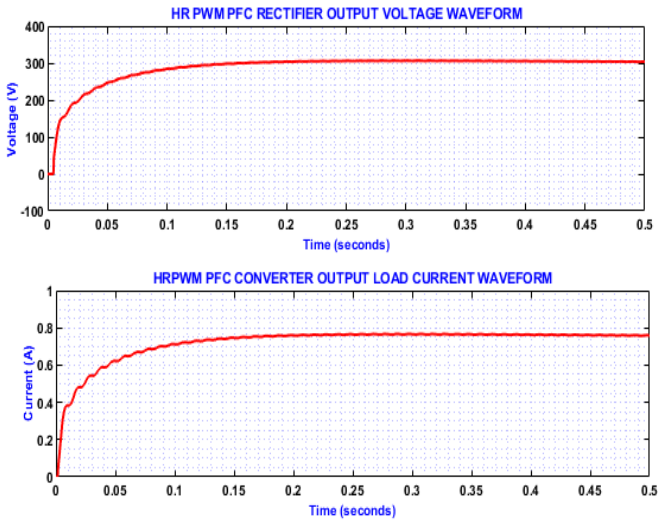

Fig. 15. Waveform for HR PWM PFC converter output current and voltage

Fig. 15 represents the HR PWM PFC converter's output current and voltage, wherever both voltage and current progressively increases and after 0.2 seconds stays consistent throughout the time period.

Case 2 → Input Voltage – 210 V

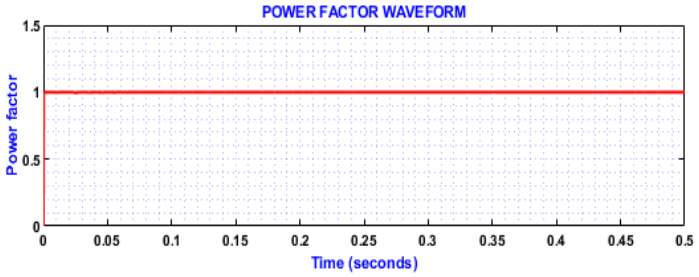

Fig. 16. Power factor

Fig. 16 indicates the power factor, which is fixed at 1 unity even with varying input voltage 210V, thereby, ensuring improved and reliable system performance.

10.22060/EEJ.2026.24491.5713

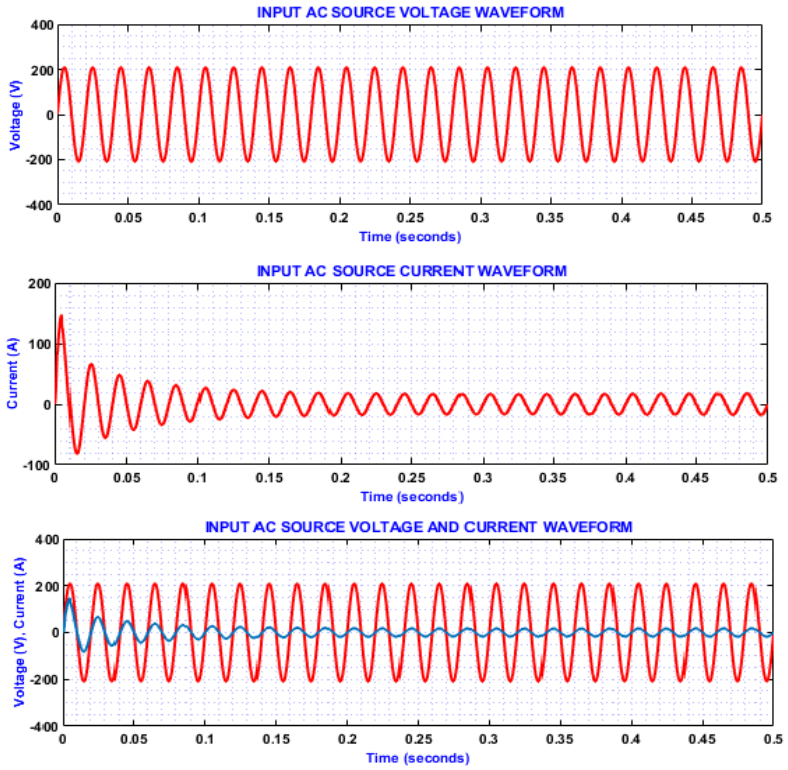

Fig. 17. AC source input voltage and current

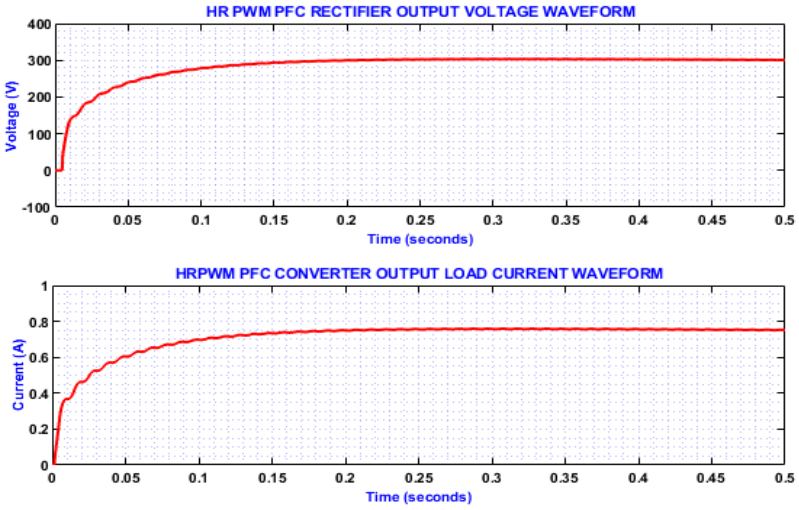

Fig. 18. HR PWM PFC converter output voltage and current

Fig. 17 implies the AC source input voltage and current, where input voltage is fixed at ±200V and current initially fluctuates and later stabilizes into steady waves. Whereas, the third graph showcases, the alignment of voltage and current, indicating unity power factor.

Fig. 18 indicates HR PWM PFC rectifier voltage on output side and converter current waveform, where the output voltage and current together progressively raises and further stabilizes after 0.2 seconds. In which the first graph displays output voltage at 300 V and the second graph shows output current at 0.7 A respectively.

Case 3 → Input Voltage – 200 V

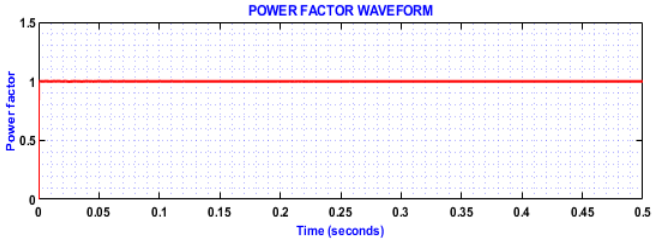

Fig. 19. Power Factor waveform

Fig. 19 represents the waveform for power factor which is fixed at 1, indicating a unity power factor throughout the given time duration even under varying input voltage 200V. Unity power factor refers that leads to reduced reactive power, indicating enhanced system functioning.

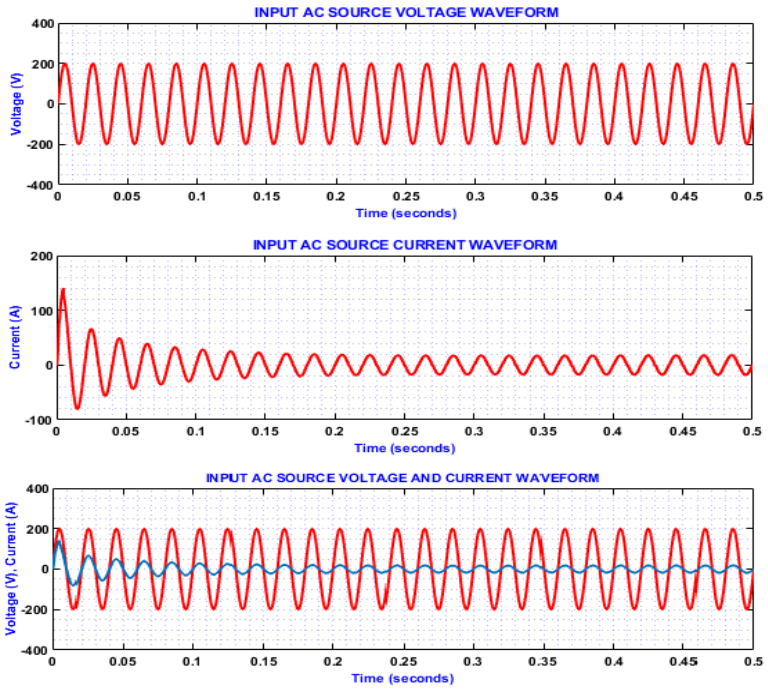

Fig. 20. Waveform of Input AC source

10.22060/EEJ.2026.24491.5713

Fig. 20 suggests the waveform for input voltage and current where, both input voltage and current remains stable and consistent for the depicted time duration and the third chart displays the combined form of both voltage and current.

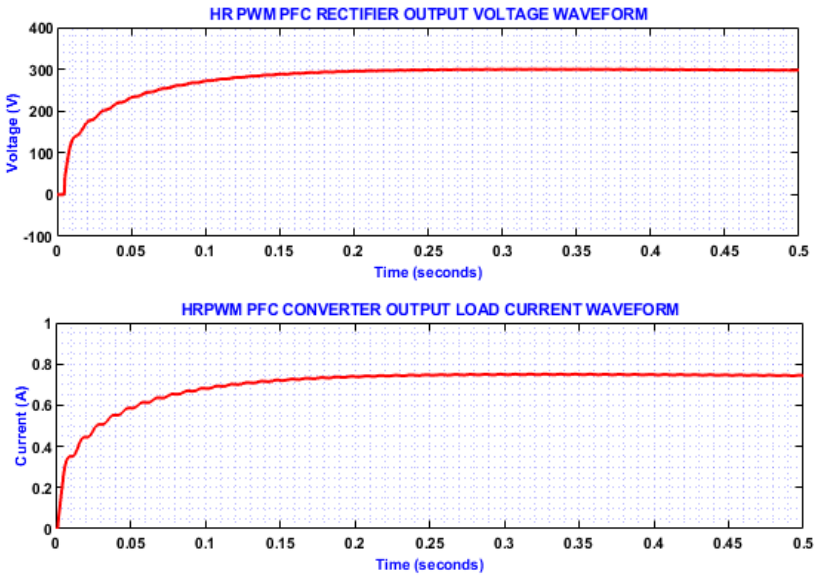

Fig. 21. Output voltage and current waveform for HR PWM PFC converter

Fig. 21 indicates the output waveform for HR PWM PFC converter, the first graph depicts the rectifier output voltage which stabilizes gradually and the second graph shows the load current output which also gradually increases and stabilizes at 0.7 A, showcasing an improved power supply. The power loss of 4.6 W is obtained from the output power of 150 W with conduction loss is nearly 65%.

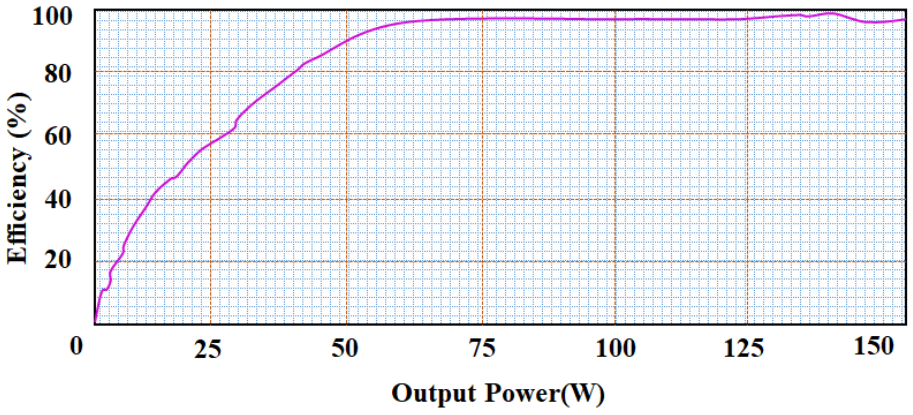

Fig. 22 Output power Vs efficiency.

An output power Vs efficiency curve is represented in Fig.22. It is concluded that the proposed converter attains the efficiency of 97%.

Table 2. Comparison of power factor correction.

Converter	Power Factor
Boost Resonant PFC converter	0.83
SEPIC Resonant PFC converter	0.86
Single Stage Resonant PFC converter	0.90
High Frequency Resonant Bridgeless PFC converter	1

Table 3. Comparison between Proposed PFC Converter with Various Conventional PFC Converters

Configuration	BL Buck Boost PFC converter [19]	BL SEPIC [22]	BL Luo [23]	BL Cuk [24]	Proposed BL Resonant PFC converter
Output Voltage Ripple	High	High	Low	Low	Low
Circuit Conduction Loss	Medium	High	Low	Low	Low
Switch Current Stress	High	High	High	High	Low
Input Current Ripple	High	Low	High	Low	Low
Output Voltage	Negative	Positive	Positive	Negative	Positive

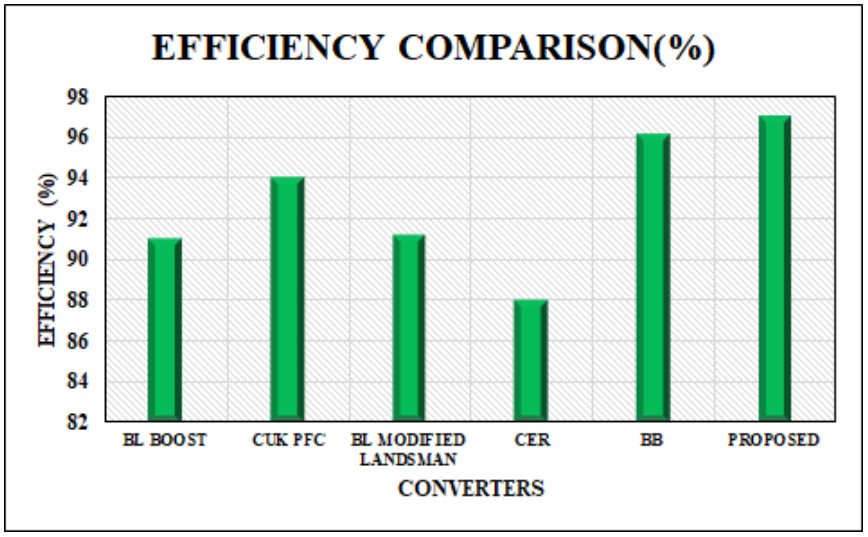

Fig. 23. Efficiency Comparison

Fig. 23 signifies the efficiency of the conventional converters with proposed converter to validate its performance efficacy, From the above chart it is evident that, the developed converter has highest efficiency of 97% while [25] BL boost, [26] BL Cuk and [27] BL modified Landsman converter attained somewhat

decreased efficacy of 91%, 94% and 91.02 % respectively. Also, the efficiency of Class E Resonant (CER) [28] and Bridgeless Boost (BB) [29] converters are 88% and 96.10%.

4. Conclusion

The proposed system concludes that, by integrating High frequency resonant bridgeless PFC converter assures increased power quality, smooth AC-DC conversion with reduced power losses. In addition to this, the utilization of PWM generator with hysteresis current controller and PI controller achieves highly regulated voltage and current, thus increasing stability and reliability with enhanced performance efficacy. Therefore, the overall proposed system ensures enhanced EV charging process with increased reliability and better EV battery performance. To validate the performance efficacy of the proposed, MATLAB/Simulink implementation is utilized, which depicts that, proposed BL PFC converter attained higher efficiency of 97% with power factor unity, indicating enhances system performance with effective EV battery charging.

References

[1] O. Dakka, S. Patthi, J. R. Rao, P. Kumar, “A 5-kW unidirectional wireless power transfer EV charger with a novel multi-level PFC boost converter on front-end side”, Journal of Engineering and Applied Science, 2024, vol. 71, no. 1, pp. 7.

[2] T. Boonraksa, P. Boonraksa, W. Pinthurat, B. Marungsri, “Optimal Battery charging schedule for a battery swapping station of an electric bus with a PV integration considering energy costs and peak-to-average ratio”, IEEE Access, 2024, vol. 12, pp. 36280-36295.

[3] N. Patel, L. A. Lopes, A. K. Rathore, V. Khadkikar, “High-Efficiency Single-Stage Single-Phase Bidirectional PFC Converter for Plug-in EV Charger”, IEEE Transactions on Transportation Electrification, 2023, vol. 10, no. 3, pp. 5636-49.

[4] K. S. Kavin, P. Subha Karuvelam, M. Devesh Raj, M. Sivasubramanian, “A Novel KSK Converter with Machine Learning MPPT for PV Applications", Electric Power Components and Systems, 2024, pp. 1-19.

[5] A. Singh, J. Gupta, B. Singh, “Bridgeless modified high-step-up gain SEPIC PFC converter based charger for light EVs battery”, IEEE Transactions on Industry Applications, 2023, vol. 59, no. 5, pp. 6155-6166.

[6] A. K. Tiwari, L. K. Sahu, M. K. Barwar, “Reliability Analysis of Multi-Level PFC Converter-Based Charger for Light EV Charging Application, Electric Power Components and Systems, 2024, vol. 52, no. 2, pp. 292-307.

[7] C. Hull, J. Wust, M. J. Booysen, M. D. McCulloch, “Techno-economic optimization and assessment of solar-battery charging station under grid constraints with varying levels of fleet EV penetration”, Applied Energy, 2024, vol. 374, pp. 123990.

[8] R. Pandey, B. Singh, “PFC-SEPIC converter-fed half-bridge LLC resonant converter for e-bike charging applications”, IET Electrical Systems in Transportation, 2020, vol. 10, no. 3, pp. 225-233.

[9] G. N. Kumar, A. K. Verma, “A single-phase interleaved buck-boost pfc based on-board ev charger”, IEEE Transactions on Industry Applications, 2023, vol. 59, no. 6, pp. 7163-74.

[10] N. Patel, L. A. Lopes, A. Rathore, V. Khadkikar, “A Soft-Switched Single-Stage Single-Phase PFC Converter for Bidirectional Plug-In EV Charger”, IEEE Transactions on Industry Applications, 2023, vol. 59, no. 4, pp. 5123-5135.

[11] A. Singh, J. Gupta, B. Singh, “Design and control of two stage battery charger for low voltage electric vehicles using high gain buck-boost PFC AC-DC converter”, IEEE Transactions on Industry Applications, 2023, vol. 59, no. 5, pp. 6125-6135.

[12] A. Dixit, K. Pande, S. Gangavarapu, A. K. Rathore, "DCM-based bridgeless PFC converter for EV charging application", IEEE Journal of Emerging and Selected Topics in Industrial Electronics, 2020, vol. 1, no. 1, 2020, pp.57-66.

[13] A. Dixit, K. Pande, S. Gangavarapu, A. K. Rathore, "Design and development of modified BL Luo converter for PQ improvement in EV charger", IEEE Transactions on Industry Applications, 2020, vol. 56, no. 4, pp. 3976-3984.

[14] R. Kushwaha, B.Singh, "Bridgeless isolated Zeta–Luo converter-based EV charger with PF preregulation", IEEE Transactions on Industry Applications, 2020, vol. 57, no. 1, pp. 628-636.

[15] J. Gupta, R. Kushwaha, B. Singh, "Improved power quality charger based on bridgeless canonical switching cell converter for a light electric vehicle", IEEE Transactions on Industry Applications, 2023, vol. 59, no. 4, pp. 4610-4619.

[16] R. Kushwaha, B. Singh, "Interleaved landsman converter fed EV battery charger with power factor correction", IEEE Transactions on Industry Applications, 2020, vol. 56, no. 4, pp. 4179-4192.

[17] A. V. Praneeth, S. S. Williamson, "A zero-voltage, zero-current transition boost cascaded-by-buck PFC converter for universal E-transportation charging applications", IEEE Journal of Emerging and Selected Topics in Power Electronics, 2020, vol. 10, no. 3, pp. 3273-3283.

[18] T. Shukla, U. K. Kalla, "A BL-CC converter-based BLDC motor drive for marine electric vehicle applications, International Transactions on Electrical Energy Systems",2022, no. 1, PP. 7026462.

[19] D. Kavitha, C. Vivekanandan, "An adjustable speed PFC buck-boost converter fed sensorless BLDC motor", International Journal of Applied Engineering Research, 2021, vol. 10, no. 20, pp. 17749-17754.

[20] E. Isen, A. F. Bakan, "Comparison of hysteresis controlled three-wire and split-link four-wire grid connected inverters", In The 8th Electrical Engineering/Electronics, Computer, Telecommunications

and Information Technology (ECTI) Association of Thailand-Conference, 2011, pp. 727-730. IEEE, 2011.

[21] A. Ghoshal, V. John, “Anti-windup Schemes for Proportional Integral and Proportional Resonant Controller”, 2010.

[22] M. V. Ewerling, T. B. Lazzarin, “Unidirectional three-phase voltage-doubler SEPIC PFC rectifier, IEEE Transactions on Power Electronics”, 2020, vol. 36, no. 6, pp. 6761-6773.

[23] R. Kushwaha, B. Singh, “Design and development of modified BL Luo converter for PQ improvement in EV charger”, IEEE Transactions on Industry Applications, 2020, vol. 56, no. 4, pp. 3976-3984.

[24] S. Dutta, S. Gangavarapu, A. K. Rathore, R. K. Singh, S. K. Mishra, V. Khadkikar, “Novel single-phase Cuk-derived bridgeless PFC converter for on-board EV charger with reduced number of components”, IEEE Transactions on Industry Applications, 2022, vol. 58, no. 3, 2022, pp. 3999-4010.

[25] K. Ashok Kumar, B. L. Narasimharaju, “Performance analysis of a bridgeless power factor correction (PFC) buck–boost LED driver with ripple diversion scheme for extended lifespan”, International Journal of Circuit Theory and Applications, 2024, vol. 52, no. 8, pp. 3870-3888.

[26] N. Sivaperumal, G. Jothimani, “An energy efficient unidirectional on-board battery charger for power factor correction in electric vehicles”, Electrical Engineering, 2024, pp. 1-16.

[27] J. Gnanavadivel, M. Shunmathi, “Single-phase front-end bridgeless modified Landsman-Canonical Switching Cell PFC converter for arc welding applications”, Automatika: časopis za automatiku, mjerenje, elektroniku, računarstvo i komunikacije, 2023, vol. 64, no. 1, pp. 104-113.

[28] H. Mahdi, A. M. Ammar, Y. Nour, M. A. Andersen, “A class-E-based resonant AC-DC converter with inherent PFC capability”, IEEE Access, 2021, vol. 9, pp. 46664-46673.

[29] Z. Chen, J. Xu, P. Davari, H. Wang, “A mixed conduction mode-controlled bridgeless boost PFC converter and its mission profile-based reliability analysis”, IEEE Transactions on Power Electronics, 2022, vol. 37, no. 8, pp. 9674-9686.